Supporting Information

The Nonlinear Relations that Predict Influenza Viral Dynamics, CD8$^+$ T cell-Mediated Clearance, Lung Pathology, and Disease Severity

Margaret A. Myers[1], Amanda P. Smith[1], Lindey C. Lane[1], David J. Moquin[2], J. Robert Michael[3], Peter Vogel[4], Stacie Woolard[5], and Amber M. Smith[1,*]

[1] Department of Pediatrics, University of Tennessee Health Science Center, Memphis, TN 38163, USA

[2] Department of Anesthesiology, Washington University School of Medicine, St. Louis, MO 63110 USA

[3] Detrus Technologies, Memphis, TN 38117, USA

[4] Department of Pathology, St. Jude Children's Research Hospital, Memphis, TN 38105, USA

[5] Flow Cytometry Core, St. Jude Children's Research Hospital, Memphis, TN 38105, USA

* amber.smith@uthsc.edu

Additional parameter ensembles

Figs S1–S2 show parameter ensembles obtained from fitting the CD8$^+$ T cell model (Eq (5)–(10)) simultaneously to viral titers and CD8$^+$ T cells from BALB/cJ mice infected with 75 $TCID_{50}$ PR8. All other parameter ensembles are shown in Fig 2 in the Main Text.

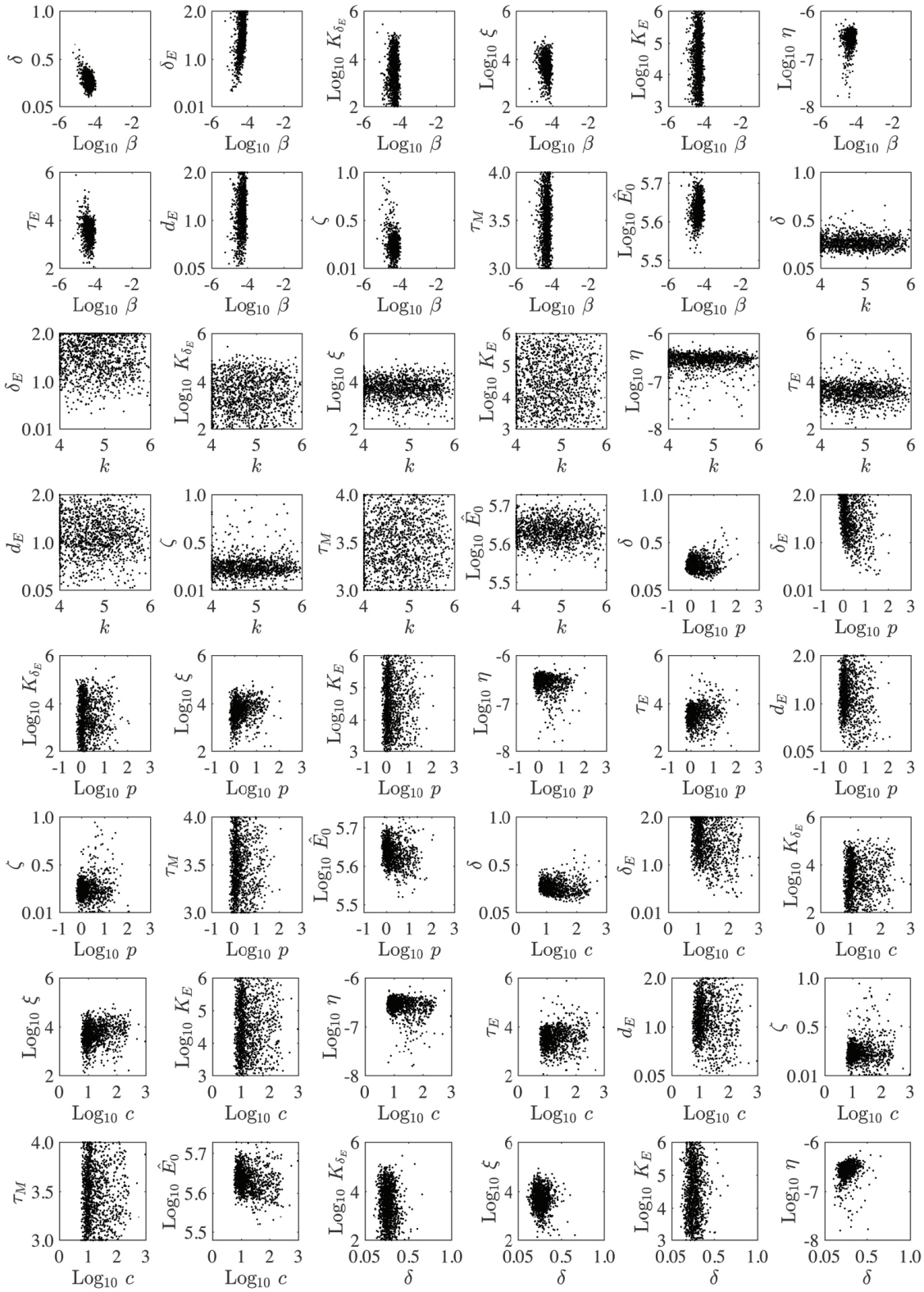

Fig S1. Parameter ensembles. Parameter ensembles resulting from fitting the $CD8^+$ T cell model (Eq (5)–(10), Main Text) to viral titers and $CD8^+$ T cells from mice infected with 75 $TCID_{50}$ PR8. The axes limits reflect the imposed bounds. Additional ensemble plots are in Fig 2A–C (Main Text) and Fig S2.

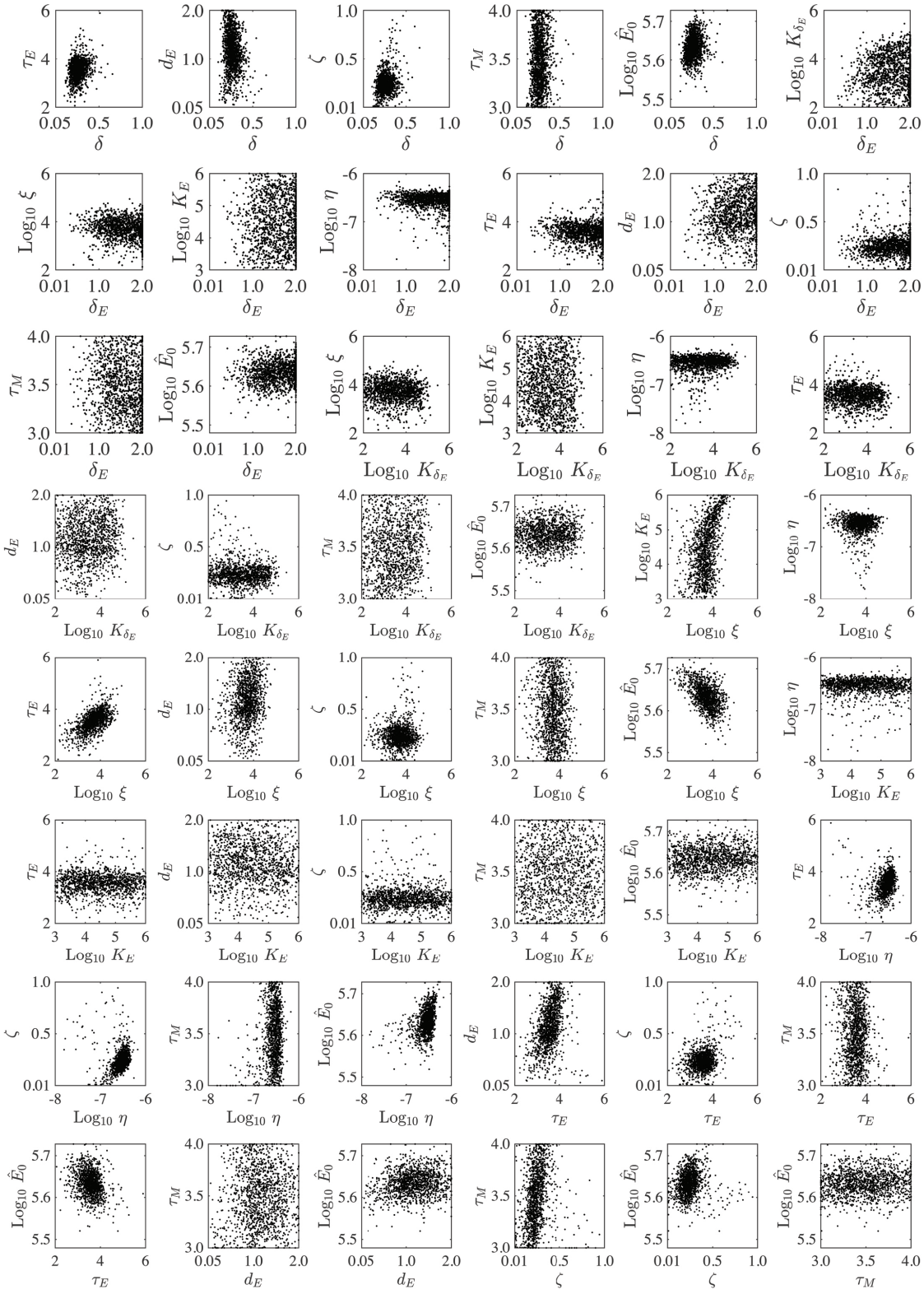

Fig S2. Parameter ensembles. Parameter ensembles resulting from fitting the CD8$^+$ T cell model (Eq (5)–(10), Main Text) to viral titers and CD8$^+$ T cells from mice infected with 75 $TCID_{50}$ PR8. The axes limits reflect the imposed bounds. Additional ensemble plots are in Fig 2A–C (Main Text) and Fig S1.

Regulation of the CD8$^+$ T cell response

To further understand the regulation of the CD8$^+$ T cell response, we examined the 2-D parameter ensembles (Fig 2A–C, Figs S1–S2) and the results from the sensitivity analysis (Fig S3–S4). Overall, few parameters were correlated. There was an expected, although small, positive correlation between the rate of $CD8_E$ infiltration (ξ) and the associated half-saturation constant (K_E) (Fig S2), which represents the coordination between $CD8_E$ recruitment and the processes that prevent an overabundance of these cells. Likewise, a negative correlation was detected between the rate of $CD8_E$ infiltration (ξ) and the initial number of CD8$^+$ T cells ($\hat{E}_0$) (Fig S2). The infiltration rate (ξ) was also positively correlated with the delay in $CD8_E$ expansion (τ_E) (Fig S2). The rates of $CD8_E$ expansion (η) and death (d_E) are correlated (Fig 2C, Main Text), indicating a balance between these two processes. This correlation was expected and reflects the coordination of mechanisms that regulate CD8$^+$ T cell numbers, which may be necessary to limit excessive immunopathology while still resolving the infection [1–3]. Further, because of this correlation and the sensitivity of η (Fig S3), the CD8$^+$ T cell kinetics are sensitive to changes in d_E (Fig S4). However, increasing the death rate had less impact on the viral load kinetics, comparatively. Because d_E is correlated with both η and the rate of $CD8_M$ generation (ζ) (Fig 2C), it naturally follows that η and ζ are correlated (Fig S2). Changing the rates of virus infectivity (β), production (p), or clearance (c) had little effect on viral load and CD8$^+$ T cell kinetics (Fig S3).

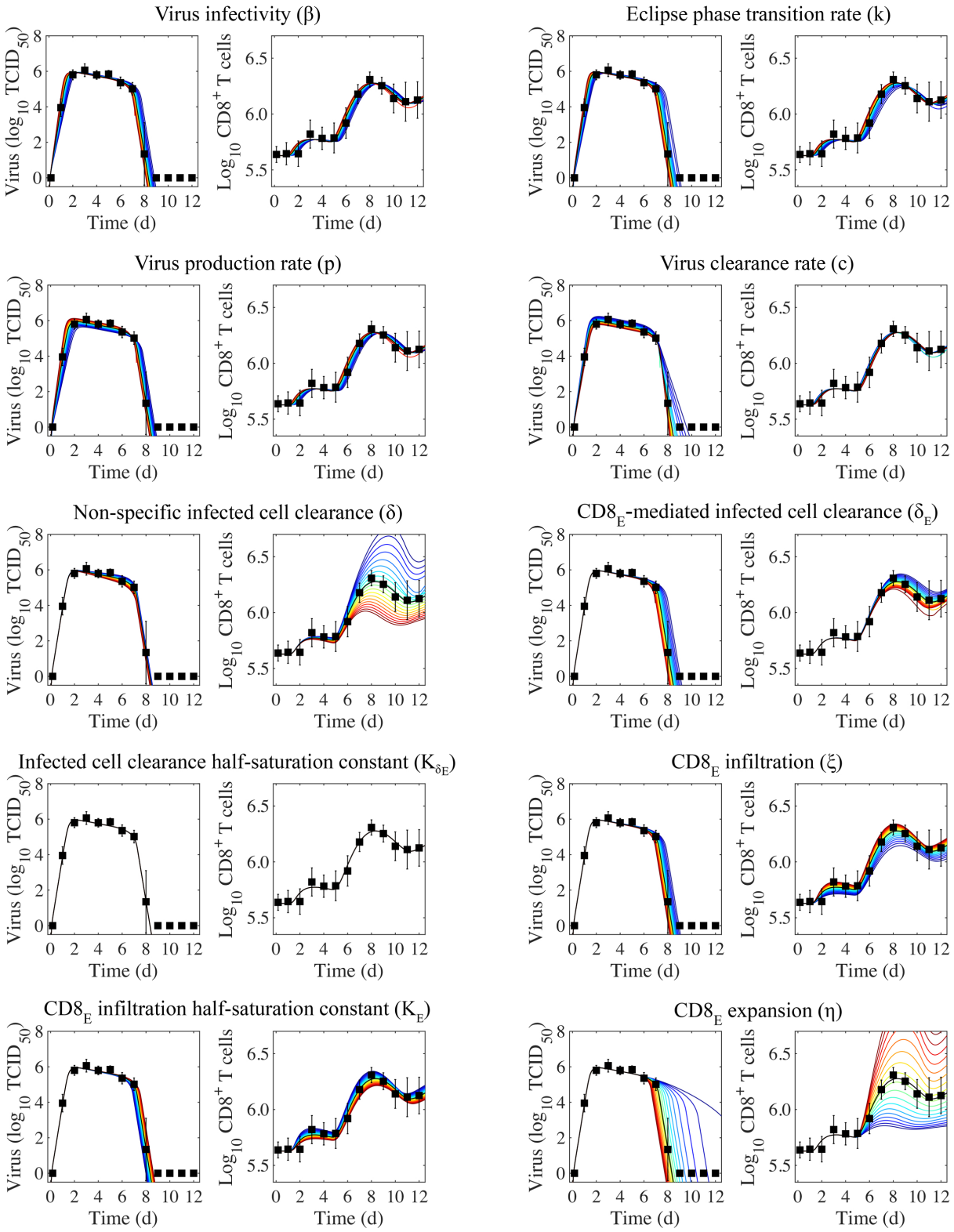

Fig S3. Sensitivity of the CD8$^+$ T cell model. Solutions of the CD8$^+$ T cell model (Eq (5)–(10); Main Text) with the indicated parameter (β, k, p, c, δ, δ_E, K_{δ_E}, ξ, K_E, or η) increased (red) or decreased (blue) 50% from the best-fit value (Table 1, Main Text). $CD8_E$ denotes effector CD8$^+$ T cells.

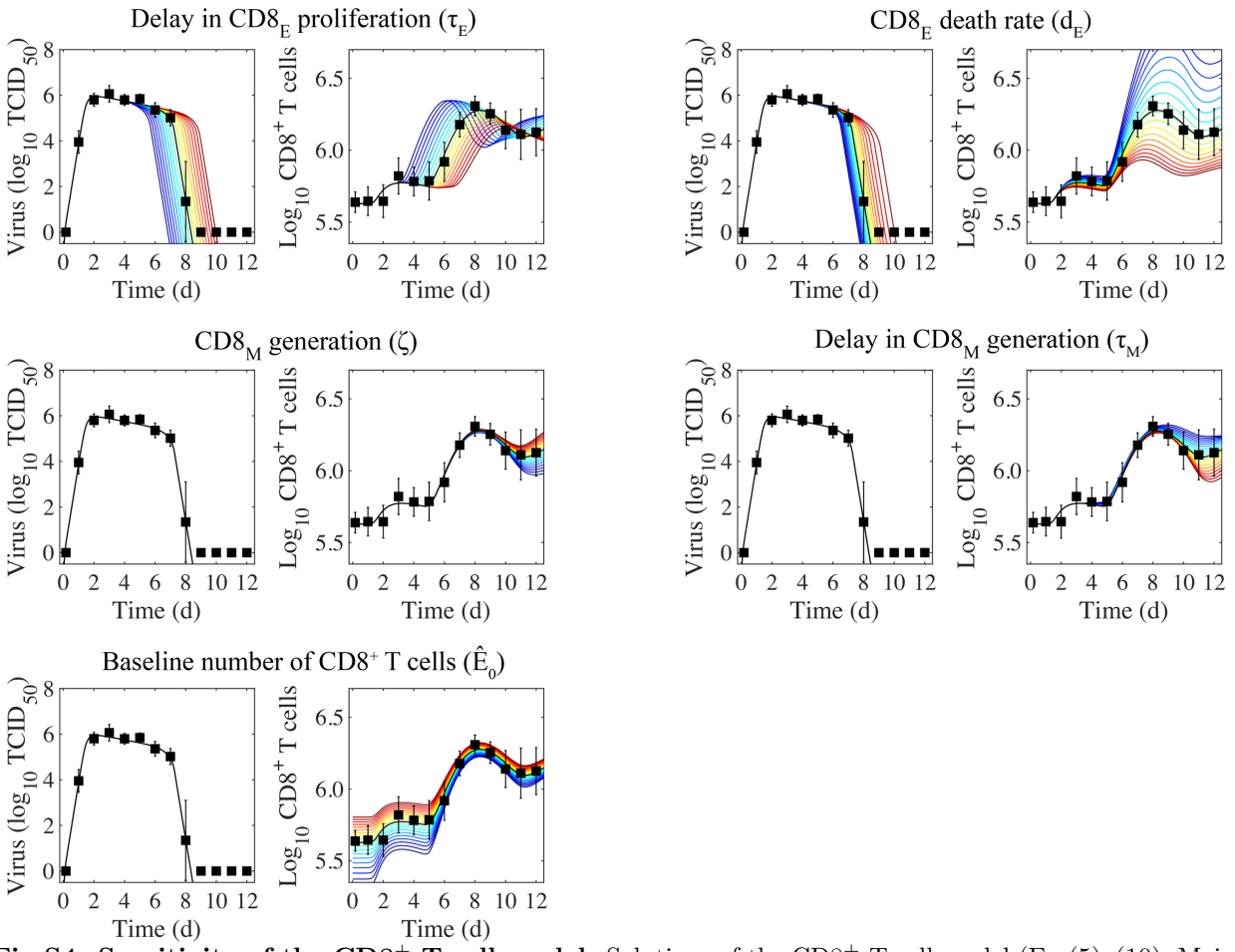

Fig S4. Sensitivity of the CD8$^+$ T cell model. Solutions of the CD8$^+$ T cell model (Eq (5)–(10); Main Text) with the indicated parameter (τ_E, d_E, ζ, τ_M, or $\hat{E}_0$) increased (red) or decreased (blue) 50% from the best-fit value (Table 1, Main Text). $CD8_E$ and $CD8_M$ denote effector and memory CD8$^+$ T cells, respectively.

Comparison of the density-dependent model and the CD8$^+$ T cell model

We previously developed and characterized the density-dependent (DD) model in Eq (1)–(4) (Main Text) [4]. The model replicates the biphasic viral load decay while excluding the dynamics of specific immune responses and assumes that the rate of infected cell clearance is dependent on their density ($\delta_d(I_2) = \delta_d/(K_\delta + I_2)$) (Fig S5). The CD8$^+$ T cell model (Eq (5)–(10), Main Text) is also capable of reproducing the biphasic viral load decay (see Fig 1B). In this model, infected cell clearance is split into terms for non-specific clearance (δ) and CD8$^+$ T cell-mediated clearance ($\delta_E(I_2, E) = \delta_E E/(K_\delta + I_2)$) (Fig S5).

Because the CD8$^+$ T cell model is more mechanistic than the DD model, most of the correlations between the parameters common to both models (i.e., the rates of virus infectivity (β), virus production (p), and virus clearance (c)) were reduced (Fig 2A). In addition, the correlations between the infected cell clearance parameters (δ_d and K_δ or δ_E and K_{δ_E}) and between the rate of virus infectivity (β) and their ratios (δ_d/K_δ or δ_E/K_{δ_E}) were abolished (Figs S1–S2). There was a negative correlation between the infected cell clearance parameters (δ and δ_E; Fig 2B), which may reflect the connection between the efficacy of early immune mechanisms and the CD8$^+$ T cell response. This result is in line with experimental evidence that the innate immune responses modulate the activation of adaptive immunity [5–9].

The differences in model structure between the two models yielded changes in parameter sensitivity and model behavior during the rapid viral clearance phase (Fig S5). In the DD model, the most sensitive

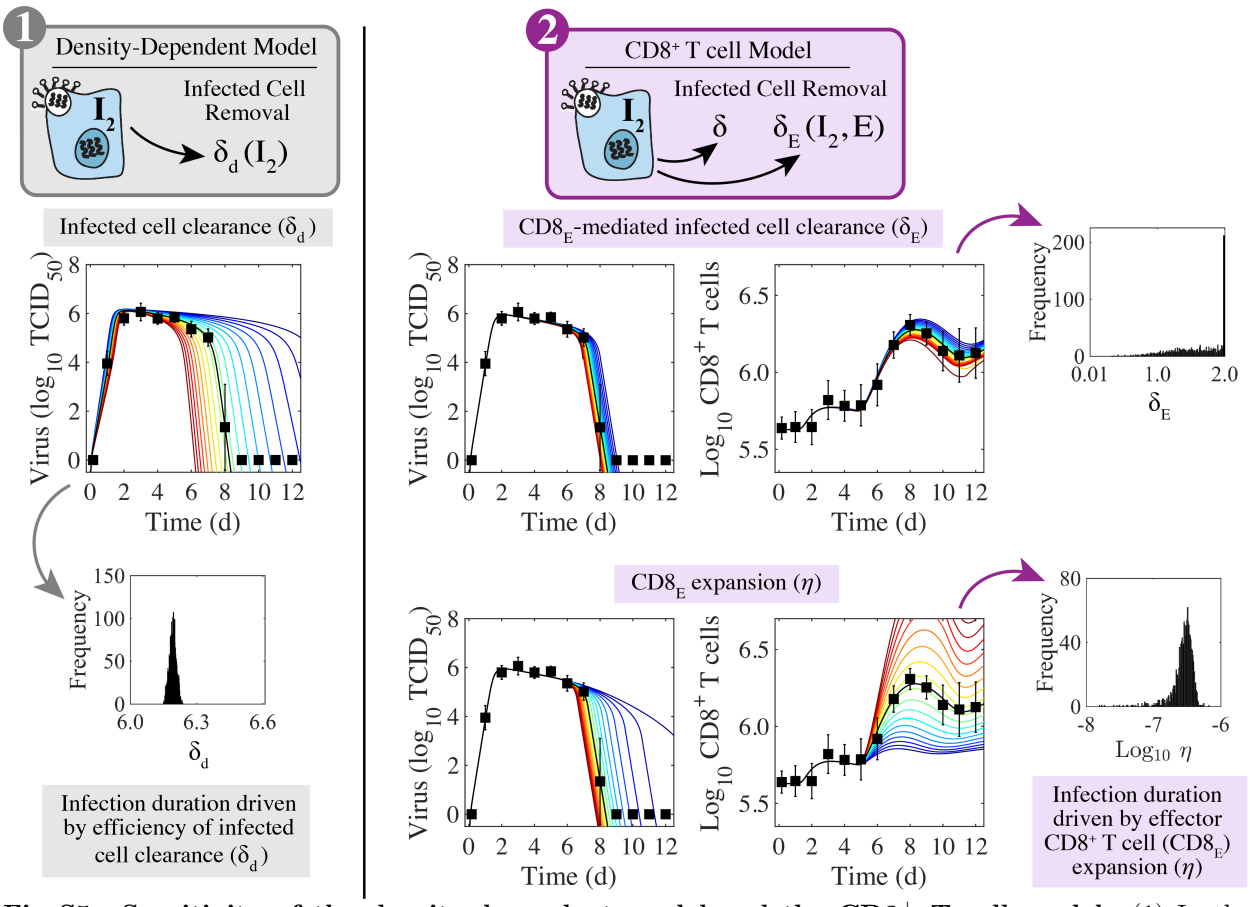

Fig S5. Sensitivity of the density-dependent model and the CD8$^+$ T cell model. (1) In the density-dependent model (gray, Eq (1)–(4)), the viral kinetics and the infection duration are sensitive to small changes in the infected cell clearance parameter (δ_d). This parameter is well-defined with a narrow 95% CI. (2) In the CD8$^+$ T cell model (purple, Eq (5)-(10)), changing the CD8$_E$-mediated infected cell clearance parameter (δ_E) has little impact on viral kinetics or CD8$^+$ T cell kinetics. However, these kinetics are most sensitive to changes in the rate of CD8$_E$ expansion (η), which is well-defined with a narrow 95% CI.

parameter is the infected cell clearance, δ_d (Fig S5). A 50% decrease in this parameter resulted in a ~7 d delay in viral resolution [4] (Fig S5). In the CD8$^+$ T cell model, however, viral resolution is delayed by <1 d if the CD8$_E$-mediated infected cell clearance parameter (δ_E) is reduced to half of its value (Figs S5–S3). The rates of CD8$_E$ expansion (η) and death (d_E) are sensitive and, thus, significantly influence the viral resolution kinetics (Figs S5–S4). A 50% decrease in η results in a ~6 d delay in recovery (Figs S5–S3) whereas a 48% decrease in η prolongs the infection by ~30 d (Fig 3D–E). This bifurcation in recovery time is a unique feature of the CD8$^+$ T cell model (discussed in the Main Text).

Linear analysis of whole lung histomorphometry

To further analyze the whole lung histomorphometry data in Fig 4, we completed a linear regression on the percent active lesioned area, the percent inactive lesioned area, and the number of CD8$^+$ T cells using the function *polyfit* in MATLAB (Fig S6). The percent active lesion declines at a rate of -28.7%/d between 6–7 d pi. The percent inactive lesion increases at a rate of 14.6%/d between 5–8 d pi, which corresponds to the increase in CD8$^+$ T cells (4.7×10^5 cells/d). The percent inactive lesion and the CD8$^+$ T cells decline at rates of -14.5%/d and -3.3×10^5 cells/d, respectively.

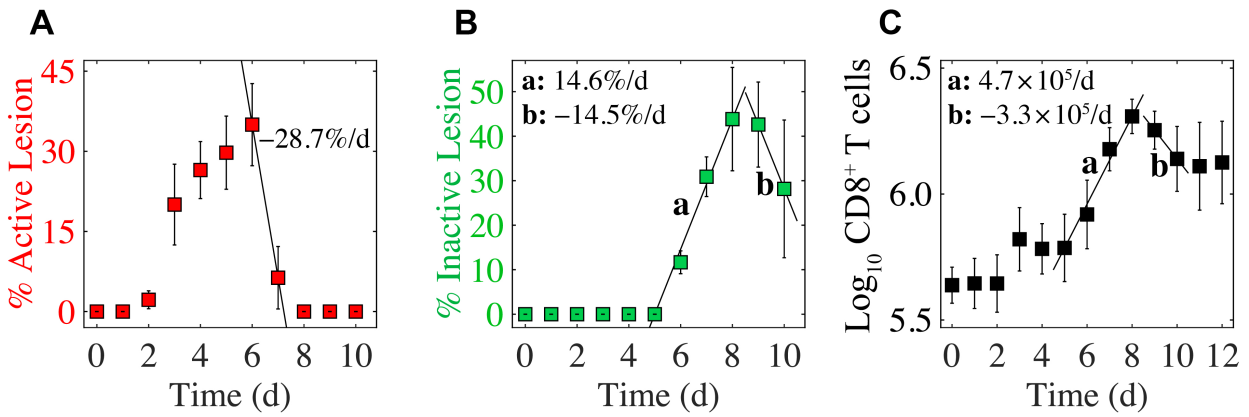

Fig S6. Linear regression analysis of whole lung histomorphometry and CD8$^+$ T cells. (A) Percent active lesion area decreases by 28.7%/d from 6–7 d pi. (B) Percent inactive lesion area increases by 14.6%/d from 5–8 d pi, and decreases by -14.5%/d from 9–10 d pi. (C) CD8$^+$ T cells increase at a rate of 4.7×10^5 cells/d (0.17 $\log_{10}$ cells/d) from 5–8 d pi, and decrease at a rate of -3.3×10^5 cells/d (-0.11 $\log_{10}$ cells/d) from 9–10 d pi.

Gating strategy for flow cytometric analysis

Fig S7 shows the gating strategy used to define CD8$^+$ T cells (Fig 1A in the Main Text). Data shown are from a representative naïve animal.

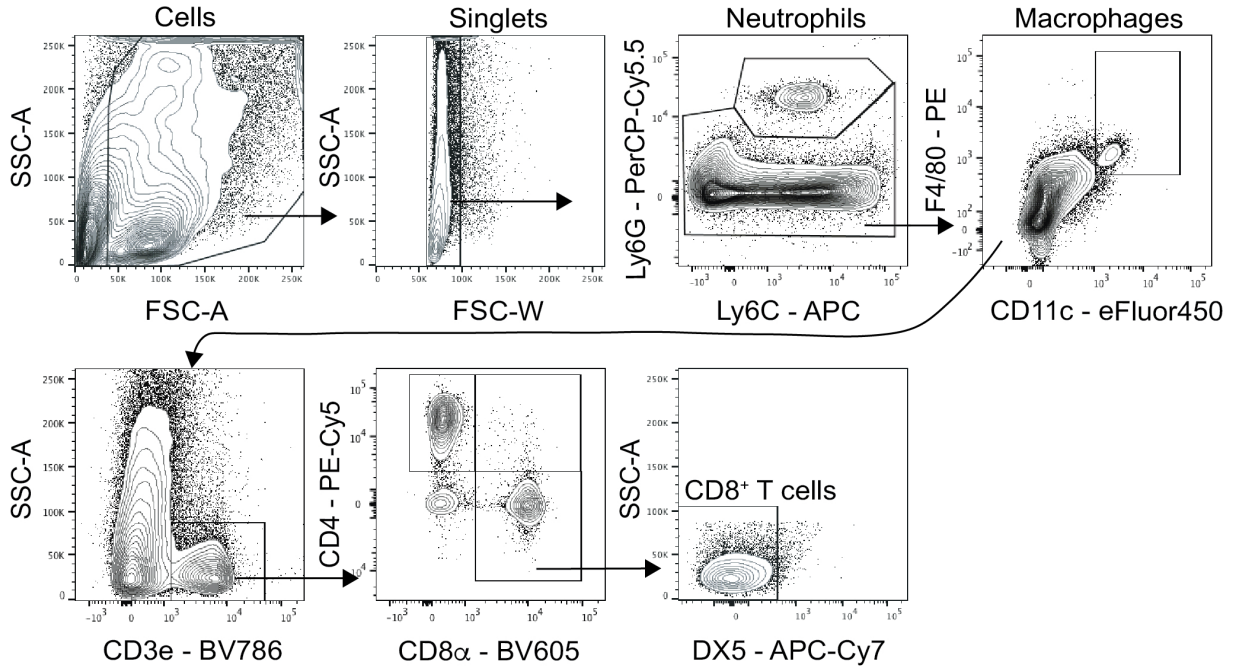

Fig S7. Flow cytometry gating strategy for CD8$^+$ T cell analysis. Live cells were first gated on forward scatter (FSC-A) and side scatter (SSC-A) then as singlets. Following neutrophil (Ly6G^{hi}) and macrophages (CD11c^{hi}F4/80^{hi}) exclusion, T cells were gated as CD3e$^+$ with CD8$^+$ T cells subgated as CD8α^+CD4$^-$DX5$^-$.

References

1. Moskophidis D, Kioussis D. Contribution of virus-specific $CD8^+$ cytotoxic T cells to virus clearance or pathologic manifestations of influenza virus infection in a T cell receptor transgenic mouse model. J Exp Med. 1998;188(2):223–232.

2. Duan S, Thomas PG. Balancing immune protection and immune pathology by $CD8^+$ T-cell responses to influenza infection. Front Immunol. 2016;7:25.

3. La Gruta NL, Kedzierska K, Stambas J, Doherty PC. A question of self-preservation: Immunopathology in influenza virus infection. Immunol Cell Biol. 2007;85(2):85–92.

4. Smith AP, Moquin DJ, Bernhaurova V, Smith AM. Influenza virus infection model with density dependence supports biphasic viral decay. Front Microbiol. 2018;9:1554. doi:10.3389/fmicb.2018.01554.

5. Iwasaki A, Medzhitov R. Control of adaptive immunity by the innate immune system. Nat Immunol. 2015;16(4):343.

6. Luster AD. The role of chemokines in linking innate and adaptive immunity. Curr Opin Immunol. 2002;14(1):129–135.

7. Iwasaki A, Medzhitov R. Regulation of adaptive immunity by the innate immune system. Science. 2010;327(5963):291–295.

8. Le Bon A, Tough DF. Links between innate and adaptive immunity via type I interferon. Curr Opin Immunol. 2002;14(4):432–436.

9. Jain A, Pasare C. Innate control of adaptive immunity: Beyond the three-signal paradigm. J Immunol. 2017;198(10):3791–3800.